

Flow Field and Heat Transfer in a Channel with a Permeable Wall Filled with Al_2O_3 -Cu/Water Micropolar Hybrid Nanofluid, Effects of Chemical Reaction and Magnetic Field

Mahdi Mollamahdi*, Mahmoud Abbaszadeh, Ghanbar Ali Sheikhzadeh

Mechanical Engineering Department, University of Kashan, Kashan, Iran

PAPER INFO

History:

Submitted 7 September 2016
Received 28 November 2016
Accepted 2 December 2016

Keywords:

Micropolar hybrid nanofluid
Magnetic field
Chemical reaction Channel
with a permeable wall
Least square method

ABSTRACT

In this study, the flow field and heat transfer of Al_2O_3 -Cu/water micropolar hybrid nanofluid is investigated in a permeable channel using the least square method. The channel encounters a chemical reaction, and a constant magnetic field also is applied. The bottom wall is hot, and coolant fluid is injected into the channel from the top wall. The effects of different parameters, such as the Reynolds number, the Hartmann number, the microrotation factor, and the concentration of nanoparticles, on the flow field and the heat transfer are examined. The results show that an increase in the Hartmann number and the Reynolds number, in turn, will increase the Nusselt and Sherwood numbers. Furthermore, when hybrid nanofluid, rather than pure nanofluid, is applied, the heat-transfer coefficient will increase significantly. It also is observed that, in the case of a generative chemical reaction, the fluid concentration is more than in the case of a destructive chemical reaction. Moreover, when the micropolar model is used, the Nusselt number and Sherwood number are less than when it is not considered.

© 2016 Published by Semnan University Press. All rights reserved.

DOI: 10.22075/jhmtr.2016.447

1. Introduction

Magneto hydrodynamics (MHD), which is concerned with the reciprocal interaction of a magnetic field and conductive fluids, is encountered in various industrial and engineering applications, such as plasma studies, electrical transformers, generators, nuclear reactors, biochemistry, and geothermal energy extraction. One of the appealing applications of MHD is the control of flow and the suppression of unsteady forces. Over the last few years, numerous researches have been devoted to the flow field and heat transfer of a fluid influenced by a magnetic field [1-8]. As early as 1986, Seth and Ghosh [9] investigated unsteady hydromagnetic flow

in a rotating channel under the influence of a periodic pressure gradient and uniform magnetic field. In a numerical study, Jha [10] examined the effect of a uniform transverse magnetic field on transient free convection flow in a channel. He observed that, as the magnetic field parameter increases, the skin friction decreases, and the time parameter increases. The impacts of the magnetic field on an unsteady flow in a channel filled with a porous medium were studied by Makinda and Mhone [11]. They indicated that increasing the magnetic field's intensity reduces wall shear stress. Pardia et al. [12] conducted a numerical investigation of MHD second-grade fluid flow in a channel with porous walls. They concluded that, in the presence of a uniform magnetic field, the radial velocity component decreases and the

induction drag increases. They also showed that the effect of viscoelastic parameters on the velocity field is more important than the effect of the Hartmann number. More recently, Nouri et al. [13] analytically studied laminar nanofluid flow in a semi-porous channel and in the presence of a transverse magnetic field. Their results showed that the velocity boundary-layer thickness decreases with an increase in the Reynolds number and nanoparticle volume fraction, and it increases as the Hartmann number increases. Fakour et al. [14] employed the least square method (LSM) to study laminar fluid flow and heat transfer in a channel with permeable walls and in the presence of a transverse magnetic field. They examined the effect of the four dimensionless numbers—the Hartmann number, Reynolds number, Prandtl number, and Eckert number—on nondimensional velocity and temperature profiles. According to their results, the velocity of the fluid decreases in the channel and the maximum amount of temperature increases when the Reynolds and Hartman numbers increase. Bovand et al. [15] conducted numerical simulations of the flow around and through a two-dimensional porous cylinder. In their study, an external magnetic field was used to control the wake behind the bluff body and also to suppress the vortex shedding phenomena. Their results show that the critical Stuart number for suppressed vortex shedding decreases with increasing Darcy numbers. In another paper, Bovand et al. [16] investigated the effects of MHD on controlling wake destructive behavior for different bluff bodies in channel flow. They concluded that the drag coefficient is reduced slowly by exerting the magnetic field at low Stuart numbers.

The analysis of improving heat transfer has been an ongoing field of research in the past few years. Nanofluids, which have better thermal conductivity than common fluids, have been proposed as a new approach to enhance heat transfer [17-19]. Even though nanofluids individually have a lot of advantages in many practical applications, another innovative approach that provides better properties and increases heat transfer in fluid flow is applying hybrid nanofluids. Hybrid nanofluids have better thermal conductivity, chemical stability, physical strength, mechanical resistance, and so on, than common nanofluids. Wang et al. [20] measured effective thermal conductivity of mixtures of fluids and nanoparticles. They used Al_2O_3 and CuO nanoparticles and water as a base fluid. They observed that the thermal conductivity of the nanoparticle–fluid mixture is higher than nanofluid.

The effect of using a water/ Al_2O_3 -Cu hybrid nanofluid in heat transfer was explored by Suresha et al. [21]. According to their results, the effective thermal conductivity of a hybrid nanofluid is greater than deionized water. Also, they measured the viscosity of the water/ Al_2O_3 -Cu hybrid nanofluid and concluded that the behavior of the viscosity of the hybrid nanofluid and Newtonian fluids is analogous. In an empirical investigation, Madhesh et al. [22] studied the heat-transfer potential of Cu- TiO_2 hybrid nanofluids in a tube-type counterflow heat exchanger. The experimental correlation for the Cu- TiO_2 hybrid nanofluid that they discovered anticipated a maximum deviation of +7% and -4% in all volume concentrations. They also demonstrated that the convective heat-transfer coefficient is augmented by 52% when hybrid nanofluids are used. Esfe et al. [23] introduced two new correlations in order to predict the thermal conductivity of a Cu/ TiO_2 -water/EG hybrid nanofluid in terms of solid concentration and temperature. The correlations are valid in different temperatures, ranging from 30°C to 60°C, and solid concentrations, ranging from 0.1 to 2%. The other researches that are dedicated to the use of hybrid nanofluid in convective heat-transfer problems are presented in [24-27].

The micropolar fluids introduced by Eringen [28] have received extensive attention in recent years due to a wide range of applications. Sheikholeslami et al. [29] employed the homotopy perturbation method (HPM) to study micropolar fluid flow in a channel by considering a chemical reaction. They examined the effects of the Reynolds number, microrotation/angular velocity, and the Peclet number on the flow and heat transfer. They observed that, for both suction and injection, the Reynolds number and Peclet number are in direct relation to the Nusselt number and Sherwood number. In an analytical investigation, Mosayebidorcheh [30] applied a new hybrid method to study the micropolar flow in a permeable channel with expanding or contracting walls. He analyzed the velocity and rotation profiles in terms of permeability, Reynolds number, rotation parameter, boundary parameter, and expanding (or contracting) ratio. He demonstrated that the profiles of the streamwise velocity and microrotation are asymmetric, while the normal velocity is symmetric. One of their applications uses the micropolar model for nanofluids in order to assess the heat transfer and find agreement between the numerical and experimental results.

The natural convection flow of a micropolar nanofluid in the presence of a magnetic field was

examined numerically by Bourantas and Loukopoulos [31] in a tilted rectangular enclosure. They demonstrated that, when the micropolar nanofluid model is used, the average Nusselt number is smaller than that of a common nanofluid model for all considered Rayleigh numbers. Also, they observed that the local Nusselt number's curve moves downward as the Hartmann number increases. Very recently, Fakour et al. [32] used the LSM to study the micropolar flow in a porous channel. They also considered the chemical reaction. They examined the effect of microrotation and the Peclet number on velocity and temperature profiles. They observed that the stream function decreases when the Reynolds number increases. Different authors have discussed micropolar fluid and nanofluid over the last two years [33-38].

Concerning LSM as an analytical solution, Sheikholeslami et al. [39] applied the Galerkin method and the LSM to study laminar flow of nanofluids in a semi-porous channel in the presence of a magnetic field. The LSM and Galerkin method are used to simulate the nanofluid flow and heat transfer in an asymmetric porous channel with expanding or contracting walls by Hatami et al. [40], and more recently, they used the LSM and numerical method to analyze the flow and heat transfer of nanofluid between contracting rotating disks [41].

As evidenced by the proliferation literature, which is mentioned above, there are no studies that could be applied to the flow and heat transfer of Al₂O₃-Cu/water micropolar hybrid nanofluid in a porous channel subject to a chemical reaction in the presence of a magnetic field. Therefore, in this study, the laminar flow of an MHD micropolar hybrid nanofluid in a channel with only a top-permeable wall that is subjected to a chemical reaction is examined through use of the LSM and the fourth-order Runge-Kutta numerical method. The conformity of the results of the least square analytical method with the Runge-Kutta numerical method is checked, and the effect of the different parameters, such as the Reynolds number, the Hartmann number, the expanding ratio, the chemical reaction parameter, and the microrotation on the heat transfer, are considered.

2. Problem statement, mathematical formulation

In the present study, the laminar flow of the MHD micropolar hybrid nanofluid in a two-dimensional channel with only a top-permeable wall

has been investigated using the LSM. The geometry of the problem is shown in Fig. 1. The bottom wall is hot and cooled by a micropolar hybrid nanofluid that is injected into the channel from the permeable top wall. The distance between the two walls is and the *x* axis, which coincides with the bottom wall. The bottom and top walls of the channel are maintained at temperatures *T*₁ and *T*₂, respectively. The thermophysical properties of water as a base fluid and Al₂O₃ and Cu nanoparticles are presented in Table 1.

Table 1. Thermophysical properties of water as a base fluid and Al₂O₃ and Cu nanoparticles [7, 42].

	$\rho(\text{kg/m}^3)$	c_p (j/kg K)	K (W/m K)	$\sigma(\Omega.m)^{-1}$	Pr
Al ₂ O ₃	3970	765	25	1×10^{-10}	-
Cu	3954	383	400	5.96×10^7	-
Pure Water	997.1	4179	0.613	0.05	6.2

The range of nanoparticles' volume fraction (90% Al₂O₃ and 10% Cu by weight) is between 0% and 2% [21]. The hybrid nanofluid density [43], heat capacity [44], electrical conductivity [45], viscosity, and thermal conductivity [21] are obtained from the following relations, respectively:

$$\rho_{nf} = (1 - \varphi)\rho_f + \varphi\rho_s, \tag{1}$$

$$\rho_{nf}c_{p,nf} = (1 - \varphi)c_{p,f}\rho_f + \varphi c_{p,s}\rho_s, \tag{2}$$

$$\frac{\sigma_{nf}}{\sigma_f} = 1 + \frac{3\left(\frac{\sigma_p}{\sigma_f} - 1\right)\varphi}{\left(\frac{\sigma_p}{\sigma_f} + 2\right) - \left(\frac{\sigma_p}{\sigma_f} - 1\right)\varphi}, \tag{3}$$

$$\frac{\mu_{nf}}{\mu_f} = -1283\varphi^2 + 8431\varphi + 0.9454, \tag{4}$$

$$\frac{k_{nf}}{k_f} = -151.5\varphi^2 + 8.916\varphi + 1.004. \tag{5}$$

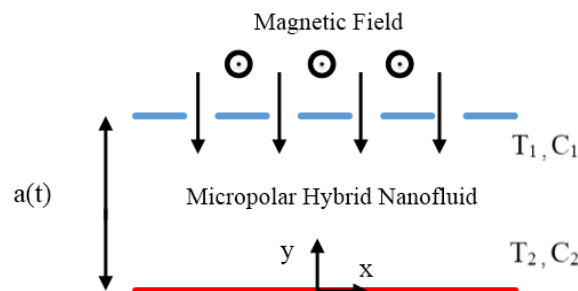


Fig.1 Schematic of the porous channel.

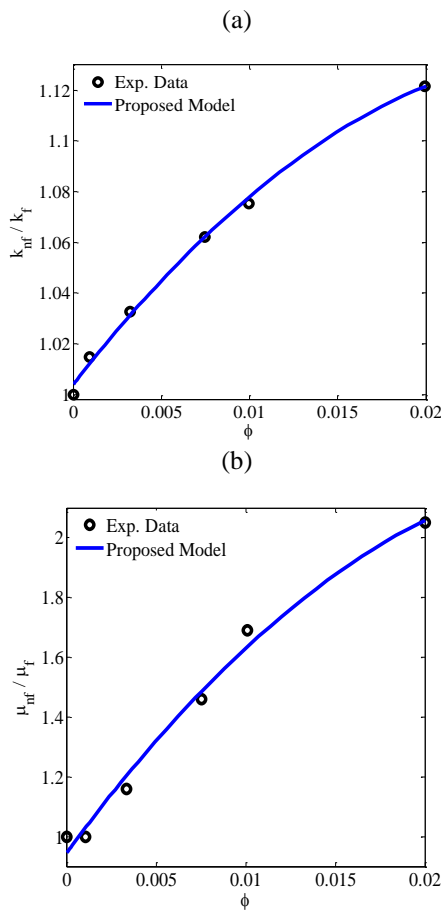


Fig.2 Proposed models for a) thermal conductivity and b) viscosity hybrid nanofluid based on the experimental data [21].

It is worth mentioning that the relations (4) and (5) are derived from an experimental model [21]. In order to correlate these relations, the experimental data has been fitted into graphs, which are depicted in Fig. 2.

The governing equations of the problem are given by [29, 46]:

$$\frac{\partial u}{\partial x} + \frac{\partial v}{\partial y} = 0, \tag{6}$$

$$\rho_{nf} \left(\frac{\partial u}{\partial t} + u \frac{\partial u}{\partial x} + v \frac{\partial u}{\partial y} \right) = -\frac{\partial P}{\partial x} + (\mu_{nf} + \kappa) \left[\frac{\partial^2 u}{\partial x^2} + \frac{\partial^2 u}{\partial y^2} \right] + \kappa \frac{\partial N}{\partial y} - \sigma_{nf} B^2 u, \tag{7}$$

$$\rho_{nf} \left(\frac{\partial v}{\partial t} + u \frac{\partial v}{\partial x} + v \frac{\partial v}{\partial y} \right) = -\frac{\partial P}{\partial y} + (\mu_{nf} + \kappa) \left[\frac{\partial^2 v}{\partial x^2} + \frac{\partial^2 v}{\partial y^2} \right] - \kappa \frac{\partial N}{\partial x}, \tag{8}$$

$$\rho_{nf} j \left(\frac{\partial N}{\partial t} + u \frac{\partial N}{\partial x} + v \frac{\partial N}{\partial y} \right) = -\kappa \left(2N + \frac{\partial u}{\partial y} - \frac{\partial v}{\partial x} \right) + \left(\mu_{nf} + \frac{\kappa}{2} \right) \left[\frac{\partial^2 N}{\partial x^2} + \frac{\partial^2 N}{\partial y^2} \right], \tag{9}$$

$$\rho_{nf} \left(\frac{\partial T}{\partial t} + u \frac{\partial T}{\partial x} + v \frac{\partial T}{\partial y} \right) = \frac{k_{nf}}{c_{p_{nf}}} \frac{\partial^2 T}{\partial y^2}, \tag{10}$$

$$\frac{\partial C}{\partial t} + u \frac{\partial C}{\partial x} + v \frac{\partial C}{\partial y} = D \frac{\partial^2 C}{\partial y^2} - k_1 (C - C_1). \tag{11}$$

where u and v are the velocity components in the x and y directions, respectively. σ , ρ , μ , c_p , j , κ , k , and N are the electrical conductivity, the fluid density, the dynamic viscosity, the specific heat at a constant pressure, the microrotation viscosity, the vortex viscosity, the thermal conductivity, and the microrotation velocity, respectively. C is the species concentration, D is the molecular diffusivity, and k_1 is the first-order chemical reaction rate. $k_1 > 0$ corresponds to the destructive reaction, $k_1 = 0$ represents no reaction and $k_1 < 0$ corresponds to the generative reaction. The boundary conditions of the problem can be expressed as follows:

$$u = 0, v = 0, T = T_1, C = C_1, N = -s \frac{\partial u}{\partial y} = 0 \quad \text{at } y = 0, \tag{12}$$

$$u = 0, v = -v_w, T = T_2, C = C_2, N = -s \frac{\partial u}{\partial y} = 0 \quad \text{at } y = a(t). \tag{13}$$

$N = 0$ represents that the microelements close to the wall are impotent to rotate. The temperature and concentration of the fluid at an η distance from the wall and the temperature of the heated wall are defined as follows:

$$T = T_1 + \sum C_m (x/a)^m \theta_m(\eta), \tag{14}$$

$$C = C_1 + \sum P_m (x/a)^m S_m(\eta). \tag{15}$$

along with the corresponding boundary conditions

$$\theta_m(0) = 1, \quad \theta_m(1) = 0; \quad (16)$$

$$S_m(0) = 1, \quad S_m(1) = 0. \quad (17)$$

When the wall temperature and species concentration are expressed as a polynomial variation (Eqs. (14) and (15)), calculating a single value for the heat-transfer coefficient along the hot wall and mass flux coefficient are not possible. Therefore, the hot wall temperature should be considered as

$$T_2 = T_1 + \sum C_m (x/a)^m \theta_m(0), \quad (18)$$

$$C_2 = C_1 + \sum P_m (x/a)^m S_m(0). \quad (19)$$

The similarity parameters are defined as:

$$u = -\frac{v}{a^2} x F_\eta(\eta, t), \quad v = \frac{v}{a} x F(\eta, t), \quad (20)$$

$$N = \frac{v}{a^3} x G(\eta, t), \quad \eta = \frac{y}{a(t)}.$$

When the above parameters are put in Eqs. (6)–(11), these equations change as follows:

$$\left(1 + \frac{q}{A_2}\right) \left(\frac{A_2}{A_1}\right) f^{(4)} - \frac{q}{A_1} g'' + 3\alpha f' + \alpha \eta f'' + (f' f'' - f f''') R - \frac{A_5}{A_1} Ha^2 f'' = 0, \quad (21)$$

$$\left(1 + \frac{q}{2A_2}\right) \left(\frac{A_2}{A_1}\right) g'' + \alpha \xi (3g + \eta g') + R \xi f' g - R \xi f g' - \frac{q}{A_2} \left(\frac{A_2}{A_1}\right) (2g - f'') = 0, \quad (22)$$

$$\theta'' = \text{Pr} \left(\frac{A_4}{A_3}\right) (-\alpha) (m\theta_m + \eta\theta') - \text{Pr} \left(\frac{A_4}{A_3}\right) R (mf'\theta + f\theta'_m), \quad (23)$$

$$S_m'' = \text{Sc}(-\alpha) (mS_m + \eta S_m') + \text{Sc}R (mf'S_m - fS_m'), \quad (24)$$

where $q = \kappa/\mu_f$, $\xi = j/a^2$. $\alpha = a\dot{a}/v_f$ is the expansion ratio, and it is positive for expansion and

negative for contraction. m is the temperature power index. The other parameters are as follows:

$$A_1 = \frac{\rho_{mf}}{\rho_f}, A_2 = \frac{\mu_{mf}}{\mu_f}, A_3 = \frac{(\rho c_p)_{mf}}{(\rho c_p)_f}, \quad (25)$$

$$A_4 = \frac{k_{mf}}{k_f}, A_5 = \frac{\sigma_{mf}}{\sigma_f}, k_2 = \frac{k_1 a^2}{\nu};$$

$$f = \frac{F}{R}, \quad g = \frac{G}{R}, \quad \text{Re} = \frac{v_w}{v_f}, \quad (26)$$

$$\text{Sc} = \frac{\nu}{D^*}, \quad \text{Ha}^2 = \frac{\sigma_f B^2 a^2}{\mu_f}.$$

It is worth noting that the Reynolds number is positive for suction and negative for injection. Sc is the generalized Schmidt number, Ha is the Hartmann number, and k_2 is the chemical reaction parameter.

The boundary conditions are

$$\theta(1) = 0, \quad f(1) = 1, \quad (27)$$

$$f'(1) = 0, \quad g(1) = 0, \quad S(1) = 0;$$

$$\theta(0) = 1, \quad f(0) = 0, \quad (28)$$

$$f'(0) = 0, \quad g(0) = 0, \quad S(0) = 1.$$

In this case the nondimensional Nusselt number and Sherwood number are given by

$$\text{Nu} = -A_3 \frac{\partial T}{\partial \eta} \bigg|_{(T_2 - T_1)} = -A_3 \theta'_m(0), \quad (29)$$

$$\text{Sh} = -\frac{\partial C}{\partial \eta} \bigg|_{(C_2 - C_1)} = -S'_m(0). \quad (30)$$

For validation of the considered numerical simulation and the LSM in this paper, the results of Sheikholeslami et al. [39] have been compared with the present study's program. It is clear that the results have good conformity (Fig. 3).

3. Analysis of the least square method

One of the approximation techniques for solving differential equations is the weighted residual method (WRM). The WRM is a general and powerful method for obtaining approximate solutions for ordinary differential equations (ODEs) or partial differential equations (PDEs). Consider the following (partial) differential equation:

$$\text{in } \Omega \quad L_m(\phi) = f, \quad (31)$$

where L_m denotes the differential operator with the highest order of derivative m in the Ω domain. ϕ is the unknown function, and f is a given function. The aim of the solution is to seek a solution of ϕ that satisfies Eq. (31).

Assume that ϕ is approximated by a function ϕ^* (trial solution), which is a linear combination of basic functions chosen from a linearly autonomous set, that is,

$$\phi \cong \phi^* = \sum_{i=1}^n c_i \varphi_i. \tag{32}$$

By substituting Eq. (32) into (31), the result of the operations generally is not f . It results in the so-called residual Rs , defined as

$$Rs = L_m(\phi^*) - f. \tag{33}$$

Some techniques are used properly to obtain an approximate function to make the residual as “small” as possible. The residual was forced to zero in an average sense by setting weighted integrals of residuals to zero. For example,

$$\int_{\Omega} Rs W_i d\Omega = 0 \quad i = 1, 2, 3, \dots, n. \tag{34}$$

Note that in the WRM, the number of weight functions W_i always equals the number of unknown constants c_i in ϕ^* . This yields n algebraic equations for the unknown constants c_i .

In the LSM, the summation of all the squares of the residues should be minimized:

$$\begin{aligned} \zeta &= \int_{\Omega} (Rs)^2 d\Omega = \sum_{i=1}^n \int_{\Omega_i} Rs_i^2 d\Omega \\ &= \sum_{i=1}^n \int_{\Omega_i} [L_m(\phi_i^*) - f_i]^2 d\Omega. \end{aligned} \tag{35}$$

In order to achieve a minimum of the functional ζ , the derivatives of ζ with respect to all the unknown parameters must be zero. That is,

$$\frac{\partial \zeta}{\partial c_i} = 2 \int_{\Omega} Rs \frac{\partial R}{\partial c_i} d\Omega = 0. \tag{36}$$

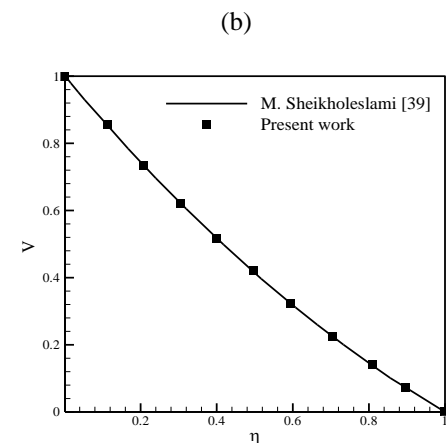
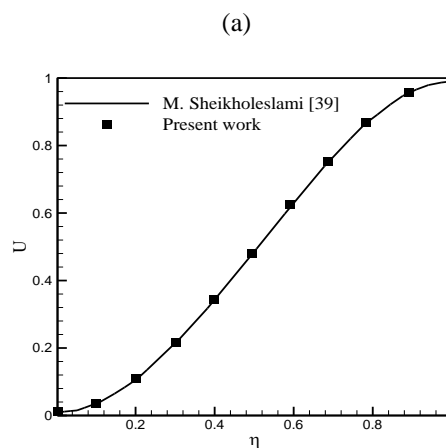


Fig. 3 Comparisons of a) velocity V and b) velocity U for $Re = 0.5$, $Ha = 0.5$, and $\phi = 0.05$.

Compared with Eq. (34), the weight functions are obtained (since its value should be zero, it is not considered constant):

$$W_i = \frac{\partial Rs}{\partial c_i}. \tag{37}$$

In order to use the LSM in this problem, the considered functions must satisfy the boundary conditions of the problem. These functions are considered generally as Eqs. (38)–(41):

$$f = y^2 + c_1(y^2 - y^3) + c_2(y^2 - y^4) + c_3(y^2 - y^5) + c_4(y^2 - y^6) + c_5(y^2 - y^7), \tag{38}$$

$$f' = 2y + c_1(2y - 3y^2) + c_2(2y - 4y^3) + c_3(2y - 5y^4) + c_4(2y - 6y^5) + c_5(2y - 7y^6), \tag{39}$$

$$g = c_6(y - y^2) + c_7(y - y^3) + c_8(y - y^4) + c_9(y - y^5), \tag{40}$$

$$q = 1 - y + c_{10}(y - y^2) + c_{11}(y - y^3) + c_{12}(y - y^4) + c_{13}(y - y^5). \tag{41}$$

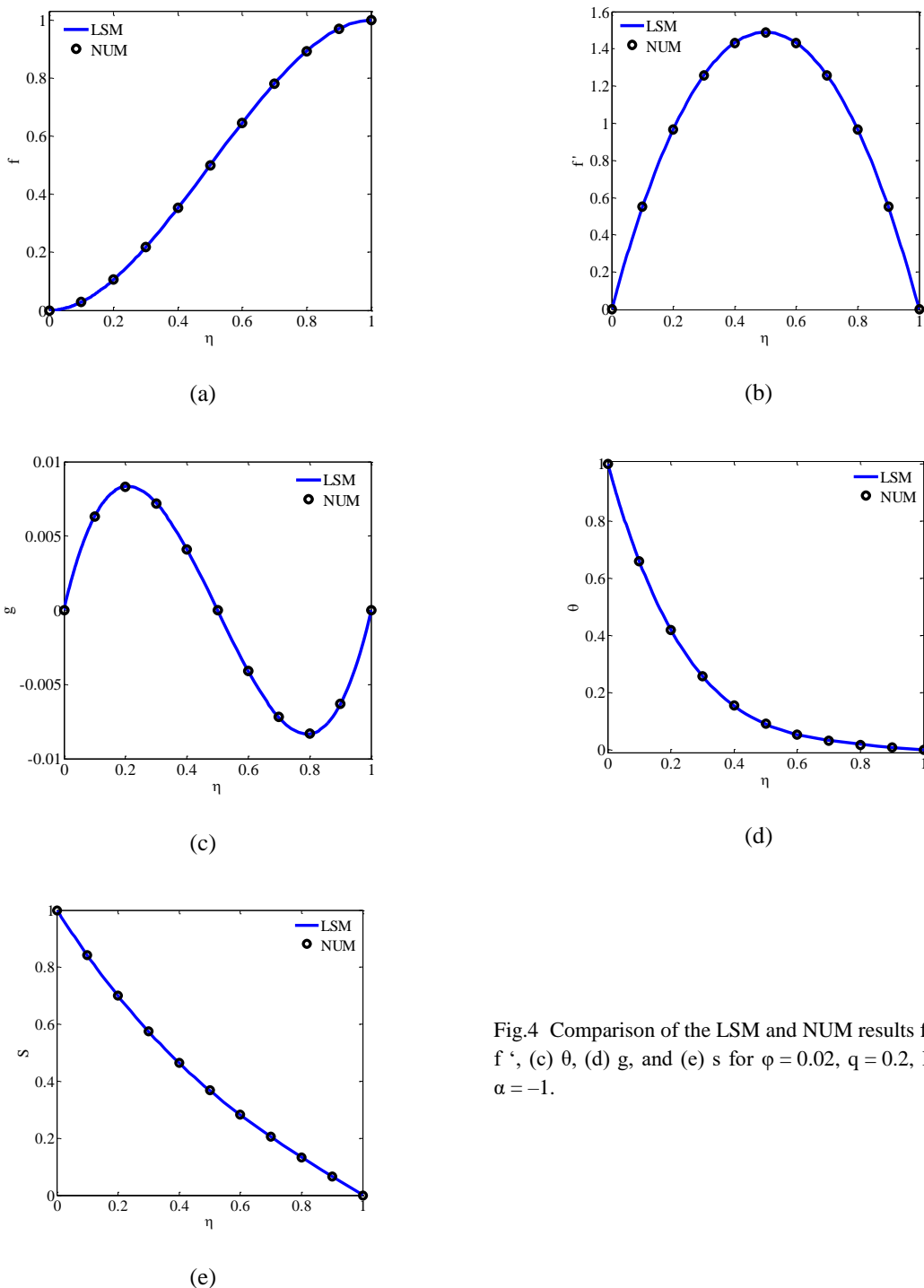


Fig.4 Comparison of the LSM and NUM results for (a) f , (b) f' , (c) θ , (d) g , and (e) s for $\phi = 0.02$, $q = 0.2$, $Re = 1$, and $\alpha = -1$.

By introducing these equations into Eqs. (21)–(24), the residual function is obtained, and by substituting the residual functions into Eqs. (38)–(41), a set of equations will be obtained. By solving these algebraic equations, coefficients c_1 – c_{13} will be determined.

4. Results and discussion

In this study, the flow field, heat transfer, microrotation, and the chemical reaction of Al_2O_3 -Cu/water micropolar hybrid nanofluid were investigated in a permeable channel with a contracting or expanding wall and in the presence of a magnetic field. The effect of using the hybrid

nanofluid was compared with common nanofluid. Also, the effects of parameters such as R , Ha , φ , q , and α on the flow field and heat transfer were examined. The study was conducted for $R = 1-7$; $Ha = 0-6$; $Sc = 0.25, 0.5, \text{ and } 1$; $k_2 = -1, 0 \text{ and } 1$; $\alpha = -1, 0, \text{ and } 1$; $q = 0.1, 0.3, \text{ and } 0.5$; $\varphi = 0.00-0.02$; $Pr = 6.2$; $m = 4$; and $\xi = 1$.

The plots in Fig. 4 indicate the components of velocity (axial velocity, f , and normal velocity, f'), temperature (θ), microrotation (g), and concentration (s), which were obtained from the LSM and numerical method (NUM) for $\varphi = 0.02$, $q = 0.2$, $R = 1$, and $\alpha = -1$. The results represent an excellent agreement between the LSM and NUM solutions. Fig. 4 illustrates the variations of microrotation in terms of η in different Reynolds numbers, α and q .

Fig. 5a shows that the microrotation diminishes near the hot wall and increases when approaching the permeable wall. With respect to the considered boundary conditions, for the microrotation parameter in this problem ($S = 0$), the microrotation value near the walls is zero. According to Fig. 4b, with an increasing α , the microrotation close to the hot wall decreases and the permeable wall increases. It is noteworthy that $\alpha > 0$ corresponds to the expanding wall and $\alpha < 0$ indicates the contracting wall. Fig. 4c represents that the increment of q leads to a microrotation increase, and the discrepancy between the maximum and minimum values of the microrotation is augmented.

In order to investigate the effect of the magnetic field on the flow field, the components of velocity (axial velocity, f , and normal velocity, f'), temperature (θ), microrotation (g), and concentration (s) in different Hartmann numbers are examined in Fig. 6. The axial velocity increases as the Hartmann number increases near the hot wall, and this behavior is reversed close to the permeable wall. In the absence of the magnetic field, the normal velocity has a maximum value in the center of the channel, while in other regions, the axial velocity is augmented when the Hartmann number increases. Moreover, with an increasing Hartman number, the temperature decreases and the concentration is augmented. Also, with augmentation of the Hartmann number, the microrotation reduces in the zone between the hot

wall and the center of the channel and increases in the spots from the center of the channel to the permeable wall.

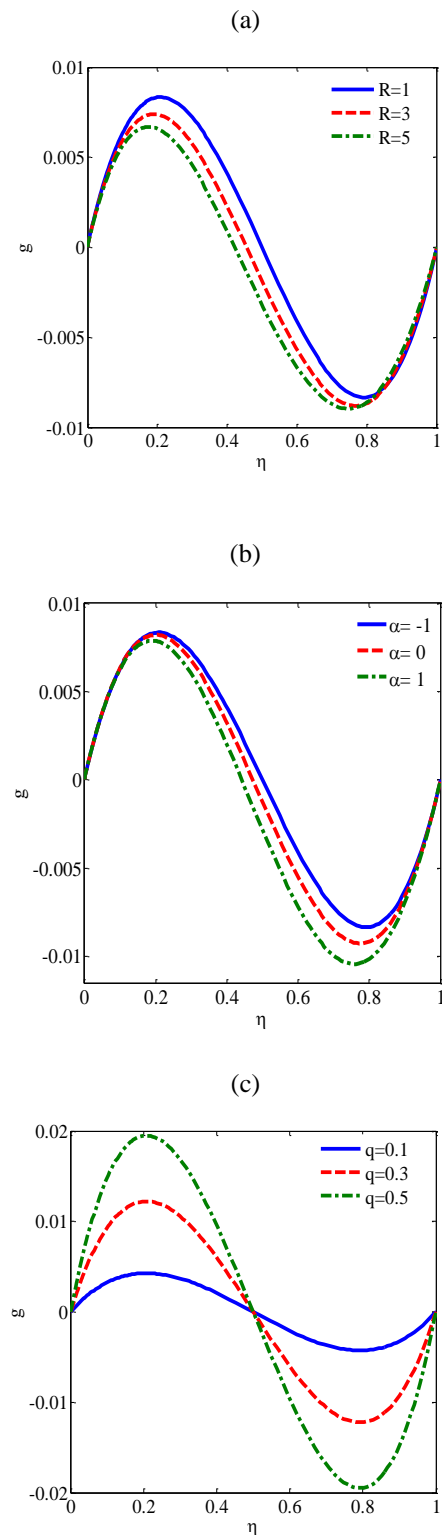


Fig.5 Variations of microrotation in terms of η in different Reynolds numbers, α and q .

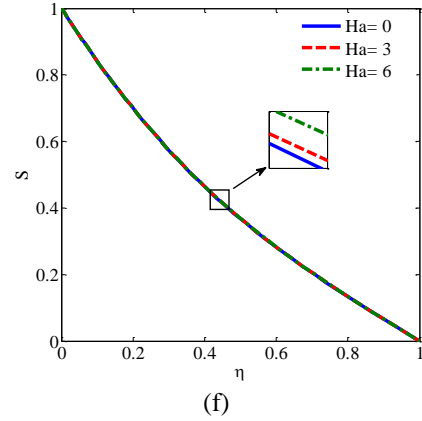
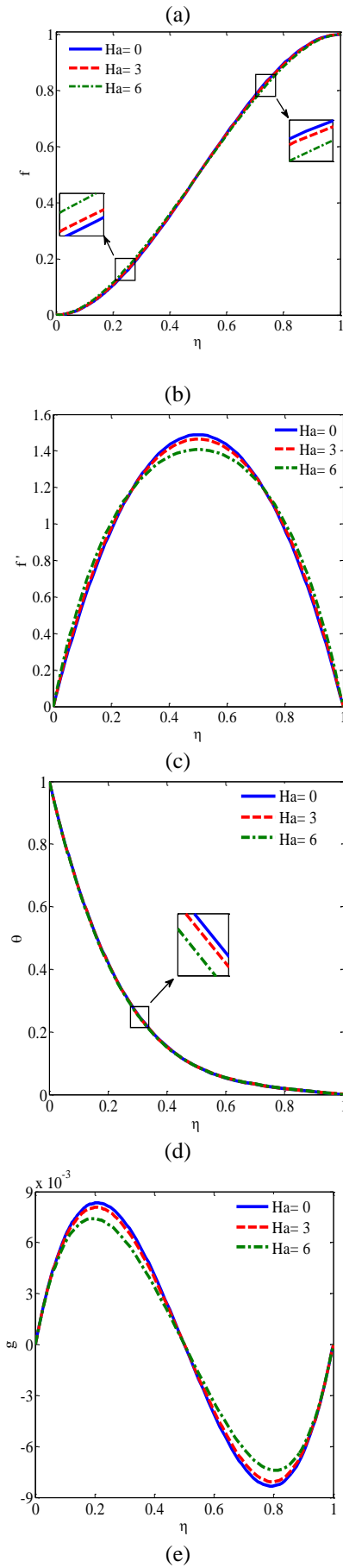


Fig.6 Effects of the Hartmann number on (a) f , (b) f' , (c) θ , (d) g , and (e) s in $\phi = 0.02$, $q = 0.2$, $Re = 1$, and $\alpha = -1$.

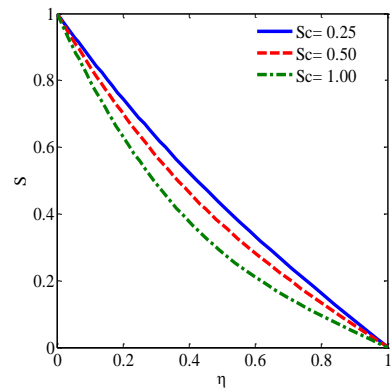


Fig.7 Effects of the Schmidt number on the concentration profile.

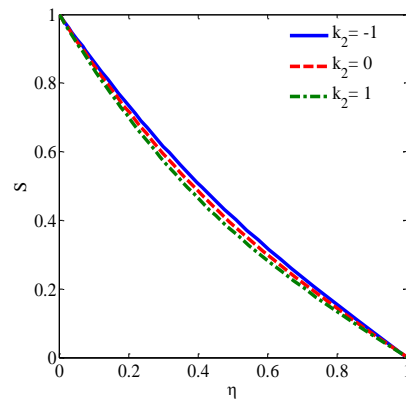


Fig.8 Effects of the chemical reaction parameter on the concentration profile.

In Fig. 7, the impact of the Schmidt number as a consequential parameter on the concentration profile is indicated. As can be seen, the fluid concentration decreases as the Schmidt number increases. To put this in perspective, Sc is the proportion of the momentum diffusivity to species diffusivity. Therefore, when the Schmidt number increases, the species diffusivity decreases and, as a result, the concentration also decreases.

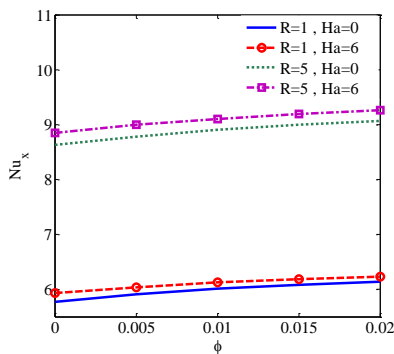


Fig.9 Variations of the Nusselt number in terms of the volume fraction with different Reynolds numbers and Hartmann numbers.

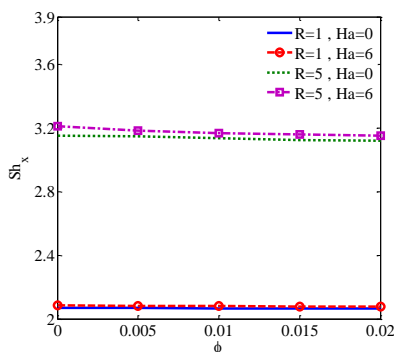


Fig.10 Variations of the Sherwood number in terms of the volume fraction with different Reynolds numbers and Hartmann numbers.

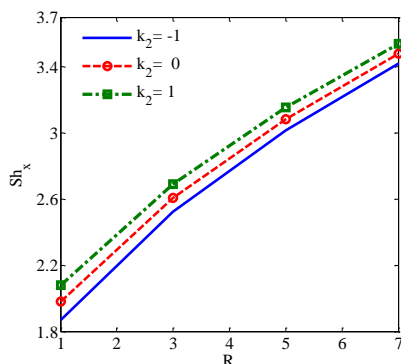


Fig.11 Variations of the Sherwood number in terms of the Reynolds number with different chemical reaction parameters.

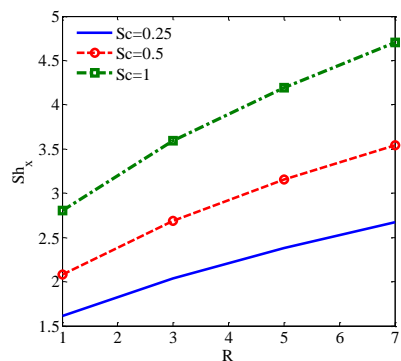


Fig.12 Variations of the Sherwood number in terms of the Reynolds number with different Schmidt numbers.

Fig. 8 elucidates the effect of the chemical reaction parameter on the concentration profile through the channel. Based on this figure, k_2 is negative for the generative chemical reaction, and k_2 is positive for the destructive chemical reaction. Fig. 9 shows variations of the Nusselt number in terms of the volume fraction in different Reynolds numbers and Hartmann numbers. As expected, with an increasing volume fraction of the nanoparticles, the Nusselt number increases. Also, with an increment in the Reynolds number and Hartmann number, the Nusselt number increases.

Variations of the Sherwood number in terms of the volume fraction in various Reynolds numbers and Hartmann numbers are depicted in Fig. 10. As seen in this figure, the volume fraction of nanoparticles, the Reynolds number, and the Hartmann number are in direct relation to the Sherwood number. Figs. 11 and 12 display variations of the Sherwood number according to the Reynolds number with different chemical reaction parameters and Schmidt numbers. It can be observed from these figures that, by increasing the Reynolds number, the Sherwood number is augmented in all k_2 and Sc . Actually, increasing the Schmidt number implies that the momentum diffusivity effect overcomes the effect of species diffusivity, and consequently, the Sherwood number increases.

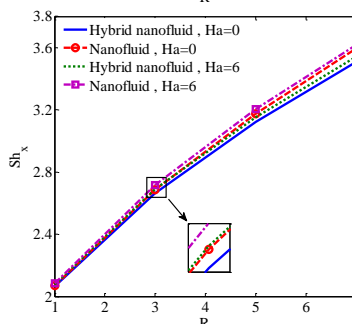
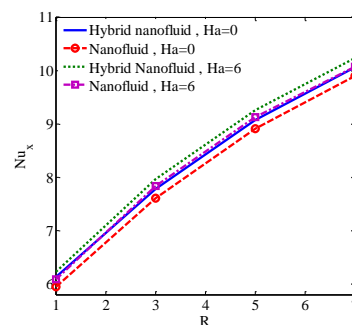


Fig. 13 Comparison of using Al₂O₃ nanoparticles and hybrid of Al₂O₃-Cu nanoparticles.

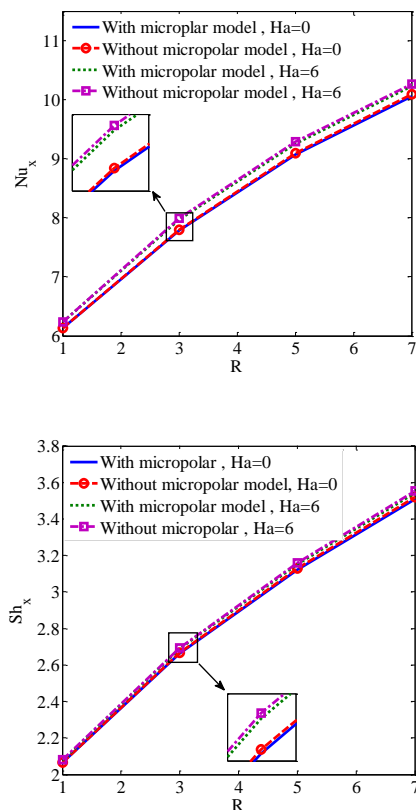


Fig.14 Comparisons of applying the micropolar model of hybrid nanofluid and the nonmicropolar model.

The plots in Fig. 13 compare the Nusselt and Sherwood numbers obtained by using Al_2O_3 nanoparticles and the hybrid of Al_2O_3 -Cu nanoparticles in different Reynolds and Hartmann numbers. Under the same circumstances, when the hybrid nanofluid is used, the obtained values of the Nusselt and Sherwood numbers are more than the common nanofluid, as a result, the heat transfer within the channel increases. Also, the properties of the nanofluid are determined using the Maxwell model [47] and Brickman model [48]. Furthermore, with increasing Hartmann and Reynolds numbers, the Nusselt and Sherwood numbers increase.

Fig. 14 represents values of the Nusselt and Sherwood numbers when the micropolar model is applied and when it is not considered in order to clarify the consequences of employing the micropolar theory. Based on this figure, when the micropolar model is considered, the Nusselt and Sherwood numbers are less than when it is not taken into account. It is worth mentioning that the micropolar theory is constructed based on experimental examination, so this effect should be considered when analyzing the flow field and heat

5. Conclusion

In this study, the flow field and heat transfer were investigated in a permeable channel occupied with Al_2O_3 -Cu/water micropolar hybrid nanofluid in the presence of a magnetic field and by considering the chemical reaction. In order to solve the governing equations, the LSM and fourth-order Runge-Kutta numerical method were applied, and a comparison between these two methods also was conducted. The effect of different parameters, such as the Reynolds number and Hartmann number on the Nusselt number and Sherwood number, was examined. Moreover, the increasing effects of employing hybrid nanofluid and the influence of applying the micropolar theory on the flow field and heat transfer were studied. The following were found based on the results:

- As the Hartman number increases, the temperature profiles decrease and the fluid concentration increases.
- In the case of a generative chemical reaction ($k_2 < 0$), the fluid concentration is greater than in the case of a destructive chemical reaction.
- When the Reynolds number increases, the Sherwood number is augmented in all chemical reaction parameters and Schmidt numbers.
- Applying a hybrid nanofluid enhances the heat transfer and the Sherwood number within the channel.
- When the micropolar model is used, the Nusselt number and Sherwood number is less than when it is not considered.

Nomenclature

C	species concentration
f	dimensionless stream function
g	dimensionless microrotation
s	dimensionless concentration
LSM	least square method
NUM	fourth-order Runge-Kutta numerical method
j	micro-inertia density
N	microrotation/angular velocity
a	distance between parallel walls (m)
$a(t)$	expand or contract function (m)
c_p	specific heat at constant pressure ($\text{Jkg}^{-1}\text{K}^{-1}$)
A_{1-5}	constant parameters in nanofluids
k	coefficient of thermal conductivity ($\text{Wm}^{-1}\text{K}^{-1}$)
k_2	first-order chemical reaction rate
k_3	chemical reaction parameter
m	temperature power index
Nu	Nusselt number
Sh	Sherwood number
P	pressure (Pa)
Pr	Prandtl number
Ha	Hartmann number
Sc	Schmidt number
q	microrotation factor

R_s	residual function
R	Reynolds number
T	temperature (k)
u, v	velocity components in x and y direction (m/s)
v_w	velocity of cooling injection fluid (m/s)
x	horizontal axis coordinate (m)
y	vertical axis coordinate (m)
<i>Greek symbols</i>	
η	similarity variable
σ	electrical conductivity ($(\Omega \text{ m})^{-1}$)
α	expansion ratio
φ	nanoparticle volume fraction
θ	dimensionless temperature
ρ	density (kgm^{-3})
μ	dynamic viscosity (Pa s)
ν	kinematic viscosity (m^2s^{-1})
κ	coupling coefficient
ϕ^*	trial function
<i>Subscripts</i>	
f	fluid
nf	nanofluid
s	solid
p	particle

Acknowledgment

The authors wish to thank the Energy Research Institute of the University of Kashan for their support regarding this research (grant no. 65473).

References

- [1]. C. E. Mehmet, B. Elif, "Natural-convection flow under a magnetic field in an inclined rectangular enclosure heated and cooled on adjacent walls," *Fluid Dynamics Research*, 38(8), (2006) pp. 564–590.
- [2]. M. Pirmohammadi, M. Ghassemi, "Effect of magnetic field on convection heat transfer inside a tilted square enclosure," *International Communications in Heat and Mass Transfer*, 36(7), (2009) pp. 776–780.
- [3]. H. Nemat, M. Farhadi, K. Sedighi, H.R. Ashorynejad, E. Fattahi, "Magnetic field effects on natural convection flow of nanofluid in a rectangular cavity using the Lattice Boltzmann model," *Scientia Iranica*, 19(2), (2012) pp. 303–310.
- [4]. H. Ashorynejad, A. A. Mohamadb, M. Sheikholeslami, "Magnetic field effects on natural convection flow of a nanofluid in a horizontal cylindrical annulus using Lattice Boltzmann method," *International Journal of Thermal Sciences*, 64, (2013) pp. 240–250.
- [5]. M. M. Rashidi, N. Vishnu Ganesh, A.K. Abdul Hakeem, B. Ganga, "Buoyancy effect on MHD flow of nanofluid over a stretching sheet in the presence of thermal radiation," *Journal of Molecular Liquids*, 198, (2014) pp. 234–238.
- [6]. M. S. Valipour, S. Rashidi, R. Masoodi, "Magnetohydrodynamics flow and heat transfer around a solid cylinder wrapped with a porous ring," *Journal of Heat Transfer*, 136(6), (2014) pp. 062601.
- [7]. A. Aghaei, H. Khorasanizadeh, G. Sheikhzadeh, M. Abbaszadeh, "Numerical study of magnetic field on mixed convection and entropy generation of nanofluid in a trapezoidal enclosure," *Journal of Magnetism and Magnetic Materials*, 403, (2016) pp. 133–145.
- [8]. S. Rashidi, J. Abolfazli Esfahani, M. S. Valipour, M. Bovand, I. Pop, "Magnetohydrodynamic effects on flow structures and heat transfer over two cylinders wrapped with a porous layer in side," *International Journal of Numerical Methods for Heat & Fluid Flow*, 26(5), (2016).
- [9]. G.S. Seth, S.K. Ghosh, "Unsteady hydromagnetic flow in a rotating channel in the presence of inclined magnetic field," *International Journal of Engineering Science*, 24(7), (1986) pp. 1183–1193.
- [10]. K. Jha, "Effects of applied magnetic field on transient free-convective flow in a vertical channel," *Indian Journal of Pure and Applied Mathematics*, 29(4), (1998) pp. 441-445.
- [11]. O. D. Makinda, P. Y. Mhone, "Heat transfer to MHD oscillatory flow in a channel filled with porous medium," *Romanian Journal of physics*, 50(9/10), (2005) pp. 931-938.
- [12]. S.K. Parida, S. Panda, M. Acharya, "Magnetohydrodynamic (MHD) flow of a second grade fluid in a channel with porous wall," *Meccanica*, 46(5), (2011) pp. 1093-1102.
- [13]. R. Nouri, D. D. Ganji, M. Hatami, "MHD nanofluid flow analysis in a semi-porous channel by a combined series solution method," *Transport Phenomena in Nano and Micro Scales*, 1(2), (2013) pp. 124-137.
- [14]. M. Fakour, A. Vahabzadeh, D.D. Ganji, "Study of heat transfer and flow of nanofluid in permeable channel in the presence of magnetic field," *Propulsion and Power Research*, 4(1), (2015) pp. 50–62.
- [15]. M. Bovand, S. Rashidi, M. Dehghan, A. J. Esfahani, M. S. Valipour, "Control of wake and vortex shedding behind a porous circular obstacle by exerting an external magnetic field," *Journal of Magnetism and Magnetic Materials*, 385, (2015) pp. 198-206.
- [16]. M. Bovand, S. Rashidi, A. J. Esfahani, R. Masoodi, "Control of wake destructive behavior for different bluff bodies in channel flow by magnetohydrodynamics," *The European Physical Journal Plus*, 131(6), (2016) pp. 1-13.
- [17]. S.U.S. Choi, "Enhancing thermal conductivity of fluids with nanoparticles," *ASME-Publications-Fed*, 231, (1995) pp. 99-106.
- [18]. C.J. Ho, M.W. Chen, Z.W. Li, "Numerical simulation of natural convection of nanofluid in a square enclosure: Effects due to uncertainties of viscosity and thermal conductivity," *International Journal of Heat and Mass Transfer*, 51(17), (2008) pp. 4506–4516.
- [19]. M. Sheikholeslami, M. M. Rashidi, D.D. Ganji, "Numerical investigation of magnetic nanofluid forced convective heat transfer in existence of variable magnetic field using two phase model," *Journal of Molecular Liquids*, 212, (2015) pp. 117-126.
- [20]. X. Wang, X. Xu, S. Choi, "Thermal conductivity of nanoparticle–fluid mixture," *Journal of Thermophysics and Heat Transfer*, 13(4), (1999) pp. 474–480.

- [21]. S. Suresha, K.P. Venkitaraj, P. Selvakumar, M. Chandrasekar, "Synthesis of Al_2O_3 -Cu/water hybrid nanofluids using two step method and its thermo physical properties," *Colloids and Surfaces A: Physicochemical and Engineering Aspects*, 388(1), (2011) pp.41–48.
- [22]. D. Madhesh, R. Parameshwaran, S. Kalaiselvam, "Experimental investigation on convective heat transfer and rheological characteristics of Cu-TiO₂ hybrid nanofluids," *Experimental Thermal and Fluid Science*, 52, (2014) pp. 104–115.
- [23]. M. Hemmat Esfe, S. Wongwises, A. Naderi, A. Asadi, M. R. Safaei, H. Rostamian, M. Dahari, A. Karimipour, "Thermal conductivity of Cu/TiO₂-water/EG hybrid nanofluid: Experimental data and modeling using artificial neural network and correlation," *International Communications in Heat and Mass Transfer*, 66, (2015) pp. 100–104.
- [24]. C.J. Ho, J.B. Huang, P.S. Tsai, Y.M. Yang, "Preparation and properties of hybrid water-based suspension of Al_2O_3 nanoparticles and MEPCM particles as functional forced convection fluid," *International Communications in Heat and Mass Transfer*, 37(5), (2010) pp. 490–494.
- [25]. S. M. Abbasia, A. Rashidib, A. Nematia, K. Arzania, "The effect of functionalisation method on the stability and the thermal conductivity of nanofluid hybrids of carbon nanotubes/gamma alumina," *Ceramics International*, 39(4), (2013) pp. 3885–3891.
- [26]. H. Balla, Sh. Abdullah, W. MohdFaizal, R. Zulkifli, K. Sopian, "Numerical Study of the Enhancement of Heat Transfer for Hybrid CuO-Cu Nanofluids Flowing in a Circular Pipe," *Journal of Oleo Science*, 62(7), (2013) pp. 533-539.
- [27]. B. Takabi, S. Salehi, "Augmentation of the Heat Transfer Performance of a Sinusoidal Corrugated Enclosure by Employing Hybrid Nanofluid," *Advances in Mechanical Engineering*, 6, (2014) pp. 147059.
- [28]. A. C. Eringen, "Theory of micropolar fluids," *Journal of Mathematics and Mechanics*, 16, (1966) pp. 1-16.
- [29]. M. Sheikholeslami, M. Hatami, D.D. Ganji, "Micropolar fluid flow and heat transfer in a permeable channel using analytical method," *Journal of Molecular Liquids*, 194, (2014) pp. 30-36.
- [30]. S. Mosayebidorcheh, "Analytical investigation of the micropolar flow through a porous channel with changing walls," *Journal of Molecular Liquids*, 196, (2014) pp. 113–119.
- [31]. G. C. Bourantas, V.C. Loukopoulos, "MHD natural-convection flow in an inclined square enclosure filled with a micropolar-nanofluid," *International Journal of Heat and Mass Transfer*, 79, (2014) pp. 930–944.
- [32]. M. Fakour, A. Vahabzadeh, D.D. Ganji, M. Hatami, "Analytical study of micropolar fluid flow and heat transfer in a channel with permeable walls," *Journal of Molecular Liquids*, 204, (2015) pp. 198–204.
- [33]. G.C. Bourantas, V.C. Loukopoulos, "Modeling the natural convective flow of micropolar nanofluids," *International Journal of Heat and Mass Transfer*, 68, (2014) pp. 35–41.
- [34]. S.T. Hussain, S. Nadeem, R. U. Haq, "Model-based analysis of micropolar nanofluid flow over a stretching surface," *The European Physical Journal Plus*, 129(8), (2014) pp. 161-171.
- [35]. M. Turkyilmazoglu, "A note on micropolar fluid flow and heat transfer over a porous shrinking sheet," *International Journal of Heat and Mass Transfer*, 72, (2014) pp. 388–391.
- [36]. E. A. Sameh, M. A. Mansour, A. K. Hussein, S. Sivasankaran, "Mixed convection from a discrete heat source in enclosures with two adjacent moving walls and filled with micropolar nanofluids," *Engineering Science and Technology, an International Journal*, 19(1), (2016) pp. 364-376.
- [37]. K. J. Sofen, K. M. Laxman, K. M. Swarup, A. J. Chamkha, "Transient buoyancy-opposed double diffusive convection of micropolar fluids in a square enclosure," *International Journal of Heat and Mass Transfer*, 81, (2015) pp. 681–694.
- [38]. Borrelli, G. Giancesio, M.C. Patria, "Magnetoconvection of a micropolar fluid in a vertical channel," *International Journal of Heat and Mass Transfer*, 80, (2015) pp. 614–625.
- [39]. M. Sheikholeslami, M. Hatami, D.D. Ganji, "Analytical investigation of MHD nanofluid flow in a semi porous channel," *Powder Technology*, 246, (2013) pp. 327-336.
- [40]. M. Hatami, M. Sheikholeslami, D.D. Ganji, "Nanofluid flow and heat transfer in an asymmetric porous channel with expanding or contracting wall," *Journal of Molecular Liquids*, 195, (2014) pp. 230-239.
- [41]. M. Hatami, M. Sheikholeslami, D.D. Ganji, "Laminar flow and heat transfer of nanofluid between contracting and rotating disks by least square method," *Powder Technonology*, 253, (2014) pp. 769-779.
- [42]. A. Arefmanesh, M. Mahmoodi, "Effects of uncertainties of viscosity models for Al_2O_3 -water nanofluid on mixed convection numerical simulations," *International Journal of Thermal Sciences*, 50, (2011) pp. 1706-1719.
- [43]. S.K. Das, S.U.S. Choi, W. Yu, T. Predeep, "Nanofluids Science and Technology," John Wiley & sons, (2008).
- [44]. Y. Xuan, W. Roetzel, "Conceptions for heat transfer correlations of nanofluids," *International Journal of Heat and Mass Transfer*, 43, (2000) pp. 3701-3707.
- [45]. AE. Jery, N. Hidouri, M. Magherbi, AB. Brahim, "Effect of an external oriented magnetic field on entropy generation in natural convection," *Entropy*, 12(6), (2010) pp. 1391–1417.
- [46]. C. Zhang, L. Zheng, X. Zhang, G. Chen, "MHD flow and radiation heat transfer of nanofluids in porous media with variable surface heat flux and chemical reaction," *Applied Mathematical Modelling*, 19(1), (2015) pp. 165-181.

[47]. J.C. Maxwell, "A Treatise on Electricity and magnetism," second ed., clarendon press, (1881).

[48]. H.C. Brinkman, "The viscosity of concentrated suspensions and solutions," *The Journal of Chemical al Physic*, 20(4), (1952) 571-571.